Graphene modulated 2D assembly of plasmonic gold nanostructure on diamond-like carbon substrate for surface-enhanced Raman scattering

ARTICLE *in* ELECTROCHEMISTRY COMMUNICATIONS · NOVEMBER 2012

Impact Factor: 4.85 · DOI: 10.1016/j.elecom.2012.09.027

6 AUTHORS, INCLUDING:

Qinghua Ren
Fudan University
4 PUBLICATIONS **28** CITATIONS
SEE PROFILE

Tang Weihua
Beijing University of Posts and Telecommu…
275 PUBLICATIONS **1,747** CITATIONS
SEE PROFILE

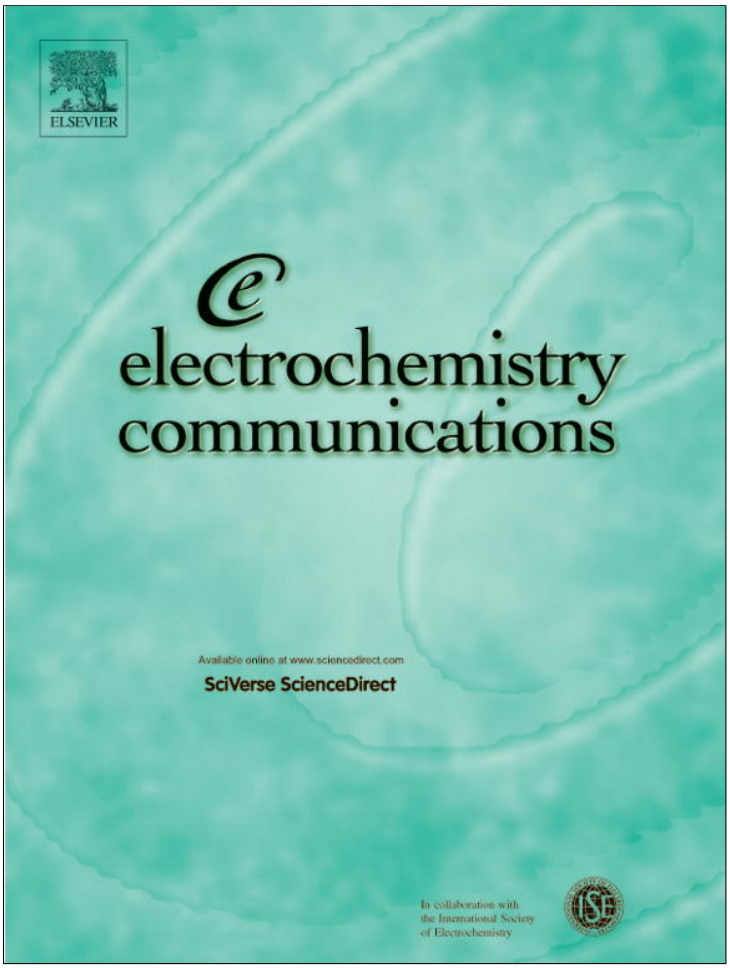

(This is a sample cover image for this issue. The actual cover is not yet available at this time.)

Electrochemistry Communications 25 (2012) 74–78

Contents lists available at SciVerse ScienceDirect

Electrochemistry Communications

journal homepage: www.elsevier.com/locate/elecom

Graphene modulated 2D assembly of plasmonic gold nanostructure on diamond-like carbon substrate for surface-enhanced Raman scattering

Aiping Liu [a,b,*], Tao Xu [a], Qinghua Ren [a], Ming Yuan [a], Wenjun Dong [a], Weihua Tang [c]

[a] Center for Optoelectronics Materials and Devices, Key Laboratory of Advanced Textile Materials and Manufacturing Technology, Ministry of Education, Zhejiang Sci-Tech University, Hangzhou 310018, China
[b] State Key Lab of Silicon Materials, Zhejiang University, Hangzhou 310027, China
[c] State Key Laboratory of Information Photonics and Optical Communication, Beijing University Posts and Telecommunications, Beijing 100876, China

ARTICLE INFO

Article history:
Received 2 August 2012
Received in revised form 14 September 2012
Accepted 17 September 2012
Available online 23 September 2012

Keywords:
Metallic plasmonics
Reduced graphene oxide
Surface-enhanced Raman scattering
Electrochemical deposition
Enhancement mechanism

ABSTRACT

A close-packed 2D assembly of plasmonic gold nanostructure was fabricated on a diamond-like carbon film by a two-step electrodeposition via reduced graphene oxide (rGO) modulation. The oxygen functionalities at the rGO surface which were controlled by changing electrochemical reduction time of GO provided reactive sites for nucleation and growth of gold nanoparticles. The Raman intensity of rhodamine B obtained from the gold assembly showed an 860-fold increase compared with that from Si reference, indicating a coupling of localized electromagnetic field enhancement and chemical enhancement. Our research offered a novel way for metallic plasmonic fabrication to realize their potential applications in biochemical analysis, environmental monitoring, disease detection and food safety.

1. Introduction

Surface-enhanced Raman scattering (SERS) is recognized as a promising analytical technique in chemical and biological detections because of its high sensitivity to low-concentration molecules adsorbed on substrates [1–3]. The SERS-active substrates have ranged from highly roughened metallic films, nanoparticle (NP) colloids to periodic nanostructures, and the NP size, shape, distribution, and the spacing between adjacent NPs affect local electromagnetic fields (known as "hot spots") in the nanoscale gap regions of coupled NPs [4–6]. Different fabrication techniques including chemical self-assembly, electrochemical deposition, photolithography and electron beam lithography have been carried out for precise control of reproducible metallic nanostructures [2,4,6–8]. However, the surfactant dosages, reaction rate and temperature need to be accurately controlled in a chemical reaction process and the resulting metallic nanostructures must be separated from heterogeneous impurities before use. The lithography techniques are used restrictedly considering the throughput and cost. The electrodeposition with simple, rapid and low-cost properties can produce well-defined metallic nanostructures with SERS-active nature [6,7] though adsorbed molecular geometries and orientations are uncontrollable on the metal surfaces. Graphene with 2D planar structure is an alternative SERS-active substrate owing to its efficient luminescence quenching for adsorbed molecules [9,10]. The graphene nanosheets combined with metallic NPs [6,11–14] show the potential predominance for low-concentration molecule detection and the oxygen functionalities at graphene surface which are related to the reduction degree of graphene oxide (GO) affect the morphologies and quantities of metallic nanostructures on graphene nanosheets [15,16]. Despite extensive experimental and theoretical efforts, the controversies about enhancement contributions from electromagnetic mechanism (EM) and chemical mechanism (CM) still exist [17,18].

In this paper, we report a graphene-mediated growth protocol to fabricate plasmonic gold nanostructures on a nitrogen doped diamond-like carbon (DLC:N) film by an electrochemical method. The DLC:N film containing sp^3- and sp^2-bonded carbon atoms is chemically stable and electrochemically active, which is suitable as the electrochemical electrode to construct gold nanostructures [19] for SERS detection [20,21]. Furthermore, the GO nanosheets are electrochemically reduced to rGO (reduced GO) to modulate the 2D assembly of gold plasmonics on DLC:N surface by a two-step electrochemical process (Fig. 1a). The effect of rGO reduction degree on the nucleation and growth of gold nanostructures is investigated. The enhancement contributions in SERS signals of rhodamine B (RhB) molecules obtained from the hybrid assembly are discussed.

* Corresponding author at: Center for Optoelectronics Materials and Devices, Key Laboratory of Advanced Textile Materials and Manufacturing Technology, Ministry of Education, Zhejiang Sci-Tech University, Hangzhou 310018, China. Tel./fax: +86 571 86843468.
E-mail address: liuaiping1979@gmail.com (A. Liu).

1388-2481/$ – see front matter © 2012 Elsevier B.V. All rights reserved.
http://dx.doi.org/10.1016/j.elecom.2012.09.027

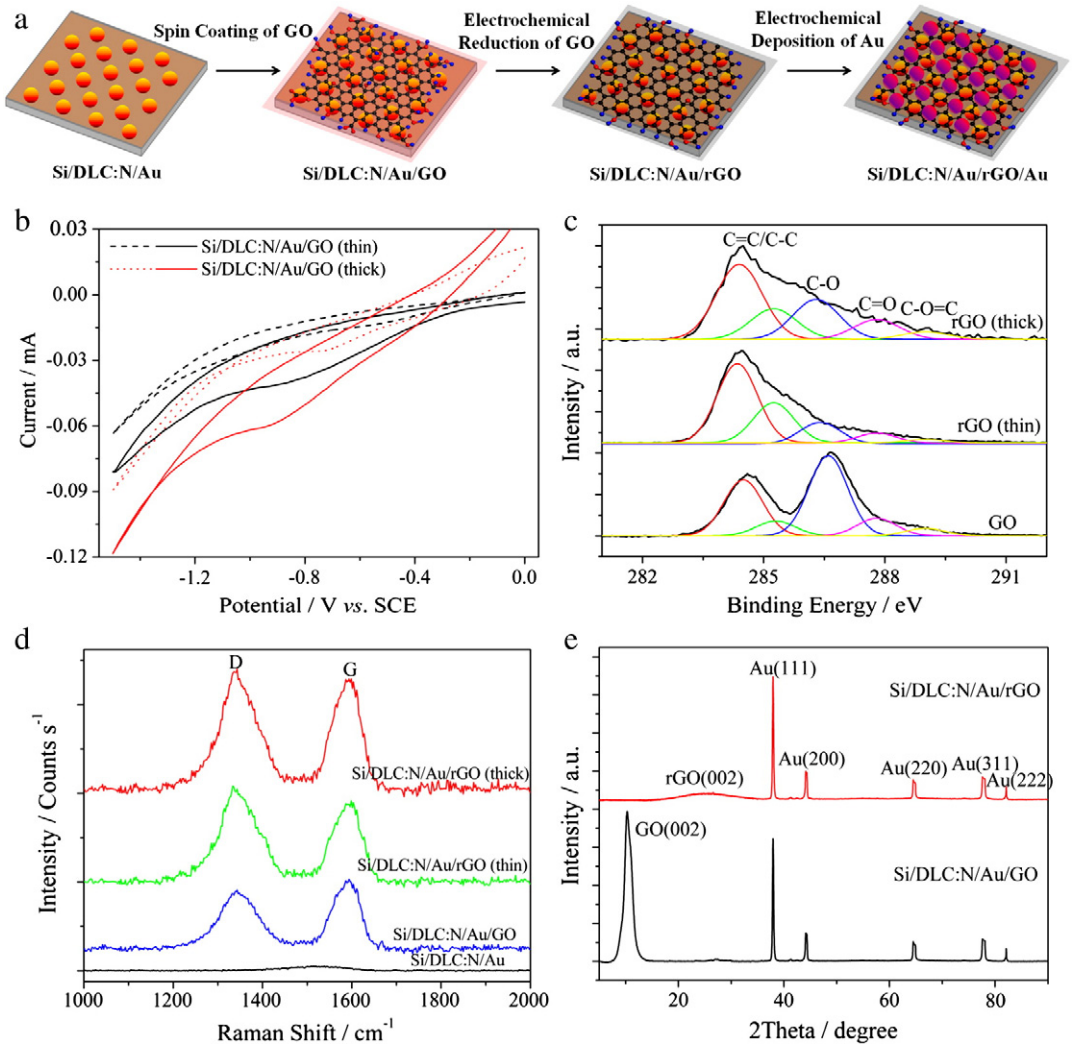

Fig. 1. (a) Schematic illustration of the fabrication of reduced graphene oxide (rGO) modulated 2D assembly of gold plasmonics. (b) Cyclic voltammograms of different-thickness GO electrochemical reduction on Si/DLC:N/Au surface. (c) C 1s spectra, (d) Raman spectra and (e) XRD patterns of GO and rGO sheets.

2. Experimental

2.1. Reagents

Graphite (50 μm) was purchased from Shanghai Carbon Co., Ltd. $HAuCl_4 \cdot 3H_2O$ (purity 99.99%) and RhB (purity 98%) were supplied by Sigma, USA. All other chemicals were of analytical grade and used without further purification. The water was obtained from a Millipore Q purification system (resistivity > 18 MΩcm).

2.2. Preparation of Si/DLC:N/Au/rGO/Au substrate

The 100-nm-thick DLC:N films (4.0 at.% N) were deposited on silicon substrates by a filtered cathodic vacuum arc system as described in literature [22]. The Si/DLC:N specimens were immersed into a 75 mM KH_2PO_4 solution containing 2 mM $HAuCl_4$ to electrodeposit gold NPs on DLC:N surfaces at −0.8 V (vs. saturated calomel electrode, SCE) for 600 s. An electrochemical workstation (CHI 630D, USA) with Si/DLC:N working electrode, SCE reference electrode and platinum foil counter electrode was used. Besides, the Si/Au and Si/DLC:N/Au specimens with 10-nm-thick magnetron-sputtered gold films were fabricated as references.

After gold NP electrodeposition, a 0.5 mg/mL exfoliated GO aqueous solution prepared by modified Hummers method [23,24] was spin-coated on Si/DLC:N/Au surfaces at 4000 rpm for 30 s and the GO thicknesses were tailored by changing GO solution volumes. The different-thickness GO were further electrochemically reduced for 10 min in a 20 mM KH_2PO_4 supporting electrolyte with the potential controlled from 0 to −1.5 V (vs. SCE) at 0.1 V/s. The secondary gold electrodeposition on Si/DLC:N/Au/rGO and Si/DLC:N/Au surfaces was then carried out at −0.8 V (vs. SCE) for different times, and the specimens were correspondingly labeled as Si/DLC:N/Au/rGO/Au and Si/DLC:N/Au/Au, respectively. The Si/DLC:N/Au(sputtering)/rGO, Si/DLC:N/Au(sputtering)/rGO/Au(electrochemistry) and Si/DLC:N/rGO/Au(electrochemistry) without primary gold loadings were prepared as the controls.

2.3. Characterization

The C 1s spectra and X-ray diffraction (XRD) patterns of GO and rGO sheets were collected by X-ray photoemission spectroscopy (XPS, KRATOS AXIS ULTRA-DLD) and a diffractometer (Bruker AXS D8) using Cu K radiation (λ = 0.15418 nm). The gold morphologies were observed by a scanning electron microscopy (SEM, Hitachi S4800). All samples for SERS measurement were incubated in the 10^{-6} M RhB aqueous solutions for 24 h to form an adsorbed monolayer and the SERS spectra were acquired with a Thermo Fisher DXR Raman spectrometer using a He–Ne laser (λ = 632.8 nm).

3. Results and discussion

3.1. Microstructures

Fig. 1b shows the cyclic voltammograms of different-thickness GO reduction on Si/DLC:N/Au surface. The cathodic current peak at about −0.9 V is attributed to oxygen group reduction of GO surfaces [25] and disappears after several scans for thin GO sheets (about 2–5 nm), hinting the quick and irreversible reduction process. For the thick GO sheets about 5–8 nm, the reduction current is higher due to more oxygen groups and the cathodic current peak is still visible after a 10 min reduction, indicating a slighter reduction of thicker GO compared to the thinner one. The C 1s spectra in Fig. 1c are decomposed into five peaks, corresponding to C═C, C–C, C–O, C═O and O–C═O bonds [22,26], respectively. The C/O atomic percentage increases from 1.66 for GO to 3.58 for thick rGO to 4.32 for thin rGO, demonstrating enhanced reduction degree from GO to rGO. This can be further deduced from Raman spectra (Fig. 1d). Compared with DLC:N with a broad Raman peak [22], the GO and rGO sheets display two prominent peaks at 1340 cm^{-1} and 1590 cm^{-1}, corresponding to D and G bands, respectively. The higher intensity ratio of D peak to G peak for thin rGO confirms the higher reduction degree of rGO with restored ordered structure [16,25,27]. The XRD patterns of GO sheets in Fig. 1e show five diffraction peaks of gold and the (002) peak of GO at $2\theta = 10.2°$, corresponding to a layer-to-layer distance d = 0.87 nm. This peak moves to $2\theta = 25.4°$ (d = 0.35 nm) after electrochemical reduction due to intercalated water molecules' elimination between neighboring rGO sheets [25].

Fig. 2 shows the gold NP morphologies of different substrates. The average size of gold NPs on Si/DLC:N surface after a 600 s deposition is about 58 nm (Fig. 2a). The thin rGO sheets on Si/DLC:N/Au surface are smooth and semi-transparent with gold nanostructures clearly distinguishable (Fig. 2b). After the second-time gold electrodeposition (600 s), the secondary gold of Si/DLC:N/Au/Au is more inclined to preferentially grow at previous gold surfaces, increasing the gold size to about 66 nm (Fig. 2c). While under rGO modulation, the secondary gold NPs renewedly nucleate and grow on the reactive sites of rGO related to oxygen-containing functional groups [15,16,28]. The small-size gold NPs formed on Si/DLC:N/Au/rGO surface with thin rGO sheets after a 30 s deposition (Fig. 2d) develop to an approximately bespreaded NP layer after a 100 s deposition (Fig. 2e), and further form a close-packed 2D assembly of gold plasmonics (Fig. 2f). The gold NPs on Si/DLC:N/Au/rGO surface with thick rGO sheets after the 30 s deposition present larger sizes and higher covering due to highly dispersed oxide groups for gold nucleation on the slighter reduced rGO (Fig. 2g) [16]. Lengthening the deposition time to 100 s does not obviously change gold-NP sizes and densities (Fig. 2h) since the sp^3 predominated network with slighter reduced rGO promotes gold NPs' dispersion along the rGO surfaces but not agglomeration [28]. Therefore, the gold nucleation at rGO surfaces might mainly be governed by oxygen groups with negative charges for Au^{3+} adsorption in the solution. Besides, the previous gold NPs below the rGO

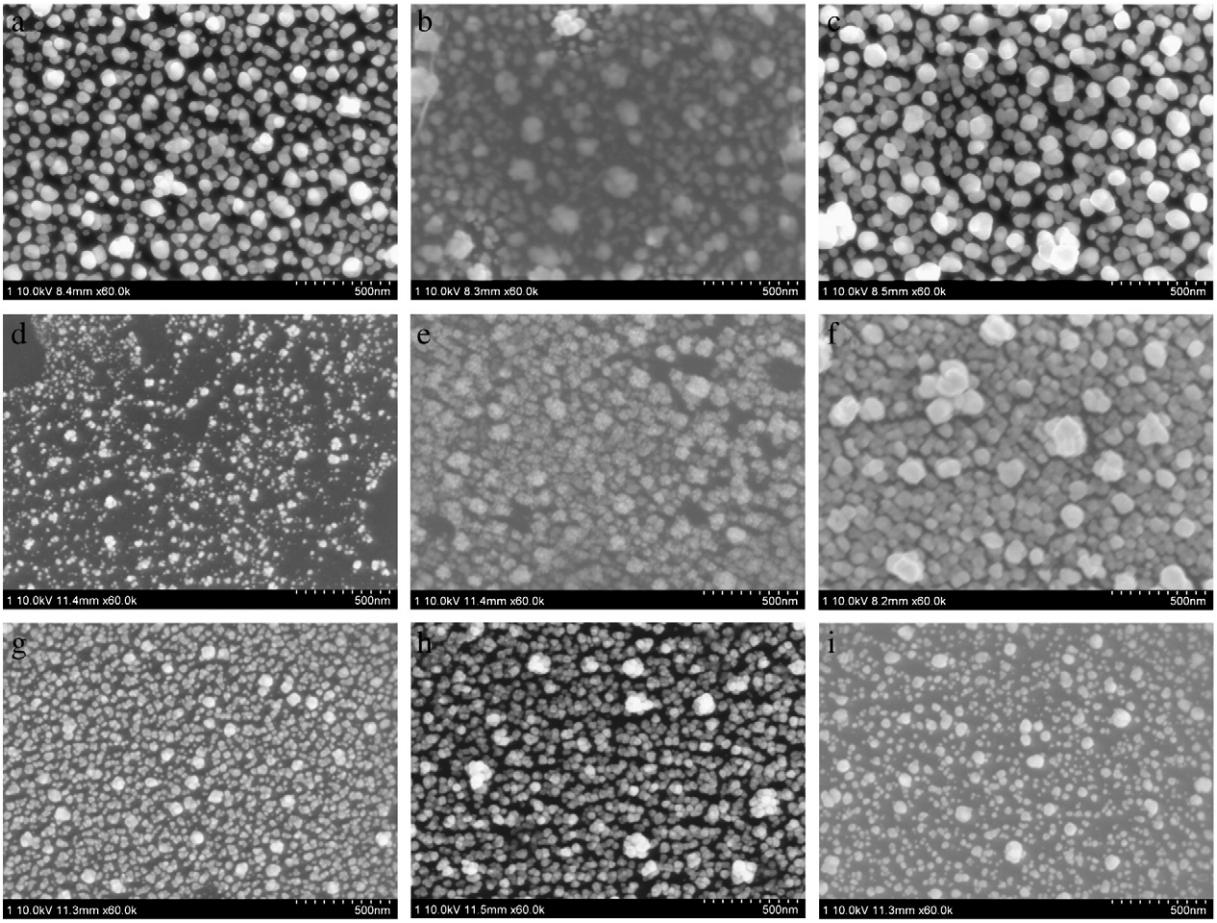

Fig. 2. SEM images of (a) Si/DLC:N/Au, (b) Si/DLC:N/Au/rGO, (c) Si/DLC:N/Au/Au, (d)–(f) Si/DLC:N/Au/rGO/Au with thin rGO sheets for (d) 30 s, (e) 100 s and (f) 600 s secondary gold electrodeposition, (g)–(h) Si/DLC:N/Au/rGO/Au with thick rGO sheets for (g) 30 s and (h) 100 s secondary gold electrodeposition, and (i) Si/DLC:N/rGO/Au with thin rGO sheets for 100 s gold electrodeposition.

sheets might also contribute to the secondary gold growth by favoring the electron transfer, forming more uniform gold assembly (Fig. 2e) compared to the Si/DLC:N/rGO/Au control (Fig. 2i) after the 100 s deposition.

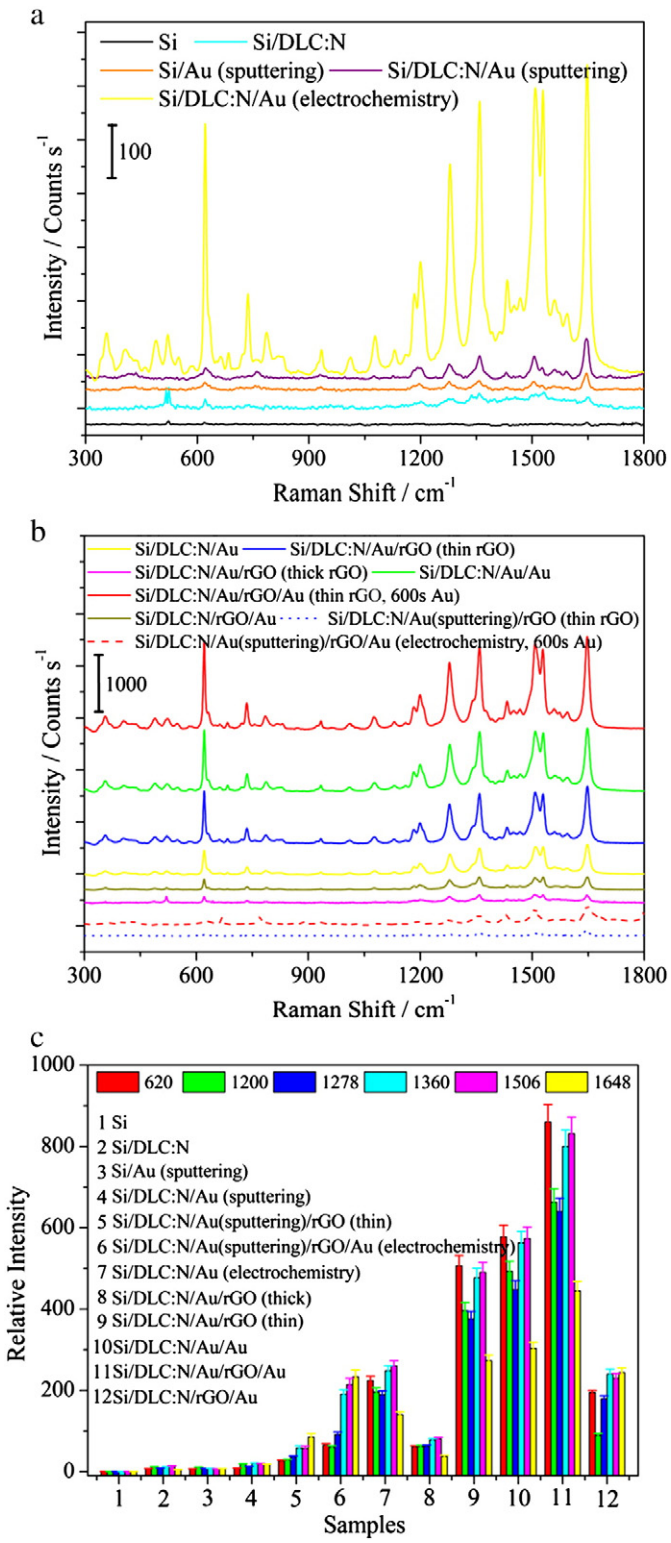

Fig. 3. (a) and (b) SERS spectra of 10^{-6} M RhB adsorbed on different substrates. (c) Relative Raman intensity of RhB adsorbed on different substrates by setting the signals on the Si substrate to "1".

3.2. SERS responses

Fig. 3 shows the SERS signals of 10^{-6} M RhB adsorbed on different substrates. Some visible Raman enhanced signals can be detected from Si/DLC:N because of the resonant Raman scattering induced by the coupling of sp^2-hybridized clusters of carbon with special sizes and probing photons. After the gold NPs' electrodepositon, the SERS signal of RhB from Si/DLC:N/Au is enlarged greatly and displays several characteristic peaks at 620 cm^{-1} (aromatic bending), 1200 cm^{-1} (aromatic C–H bending), 1278 cm^{-1} (C–C bridge-bands stretching), 1360 cm^{-1} (aromatic C–C stretching), 1506 cm^{-1} (aromatic C–C stretching) and 1648 cm^{-1} (aromatic C–C stretching) (Fig. 3a) [4]. This obvious enhancement in Raman signal can be interpreted as the dramatic change of localized electromagnetic field of gold with DLC:N layer [20,21]. The magnetron-sputtered gold films are not beneficial to Raman signal enhancement due to more smooth surfaces compared to gold NPs. To our surprise, the Raman signal of RhB obtained from Si/DLC:N/Au/rGO with thin rGO sheets is obviously enhanced by up to 500 times compared to that from electrochemically fabricated Si/DLC:N/Au (260-fold increase) by setting the signal on the Si substrate to "1" (Fig. 3b and c). This might be due to the diplex effects of intense localized electromagnetic fields created by surface plasmon polaritons at gold NPs [5,8] and the charge transfer between close aromatic molecules and rGO nanosheets due to their energy gap matching [9]. However, the Raman amplification degree is weakened dramatically as rGO thickness increases due to the "first-layer effect" of CM based on rGO [9,12]. After the secondary gold electrodeposition, the rGO modulation makes gold NPs realign to form close-packed 2D assembly. The junction areas between adjacent NPs generate plasmon resonances or "hot spots", giving rise to more intense and localized electromagnetic fields than dispersed NPs when excited by incident laser [5]. This might be most responsible for the enhanced Raman signal by up to 860 times for Si/DLC:N/Au/rGO/Au with thin rGO after 600 s electrodeposition (Fig. 3c). Besides, the electron donation from rGO layers to Au NPs (p-type doping effect) might produce more negatively charged gold NPs and prefer adsorb positively charged RhB molecules, resulting in higher SERS selectivity [12]. Notice that an interlayer electric field in the out-of-plane direction might be formed on the Au/rGO/Au sandwich structure when rGO sheets could be corrugated [14]. In our present result, the in-plane polarization between adjacent NPs might play a main role for the SERS signal, which gives a reasonable explanation for the comparatively weak signal obtained from Si/DLC:N/rGO/Au control due to the dispersed gold NPs on it. Besides, the weaker SERS signals obtained from Si/DLC:N/Au(sputtering)/rGO/Au(electrochemistry) and Si/DLC:N/Au(sputtering)/rGO controls compared to the Si/DLC:N/Au/rGO/Au and Si/DLC:N/Au/rGO samples with electrodeposited gold NPs also hint the important role of previous gold NPs below the rGO sheets in the Raman signal enhancement, which is consistent with the reported result of Kim et al. [14].

4. Conclusions

A 2D assembly of plasmonic gold nanostructure was prepared on a nitrogen doped diamond-like carbon (DLC:N) film by an electrochemical method under reduced graphene oxide (rGO) modulation. The size and density of gold nanoparticles depended principally on the oxygen functionalities at the rGO surface related to rGO reduction degree. The fabricated Si/DLC:N/Au/rGO/Au was directly used as a highly SERS-active substrate for rhodamine B molecule detection in terms of a near-field coupled electromagnetic enhancement caused by close-packed gold plasmonics as well as chemical enhancement induced by the charge transfer between close aromatic molecules and fewer-layered rGO nanosheets. The novel, simple, fast and low-cost fabrication process favored the 2D plasmonic metallic nanostructure a dramatic SERS sensitivity for rhodamine B detection,

which was valuable for hybrid assembly application in nano-optical devices, and molecule-level detectors and sensors.

Acknowledgments

This work was supported by the National Natural Science Foundation of China (51272237, 50902123 and 51172208), the Visiting Scholars Fund of State Key Lab of Silicon Materials, Zhejiang University (SKL2011-20), the Qianjiang Talent Program of Zhejiang Province (QJD1102007), and the Excellent Young Talents Foundation of Key Laboratory of Advanced Textile Materials and Manufacturing Technology (Zhejiang Sci-Tech University) (2011QN05).

References

[1] S.M. Nie, S.R. Emery, Science 275 (1997) 1102.
[2] C. Fang, A. Agarwal, K.D. Buddharaju, N.M. Khalid, S.M. Salim, E. Widjaja, M.V. Garland, N. Balasubramanian, D.L. Kwong, Biosensors & Bioelectronics 24 (2008) 216.
[3] S. Grutzke, S. Abdali, W. Schuhmann, M. Gebala, Electrochemistry Communications 19 (2012) 59.
[4] J.T. Zhang, X.L. Li, X.M. Sun, Y.D. Li, The Journal of Physical Chemistry. B 109 (2005) 12544.
[5] J.B. Lassiter, J. Aizpurua, L.I. Hernandez, D.W. Brandl, I. Romero, S. Lal, J.H. Hafner, P. Nordlander, N.J. Halas, Nano Letters 8 (2008) 1212.
[6] Y. Hu, L.H. Lu, J.H. Liu, W. Chen, Journal of Materials Chemistry 22 (2012) 11994.
[7] Y.C. Tsai, P.C. Hsu, Y.W. Lin, T.M. Wu, Electrochemistry Communications 11 (2009) 542.
[8] F.S. Ou, M. Hu, I. Naumov, A. Kim, W. Wu, A.M. Bratkovsky, X.M. Li, R.S. Williams, Z.Y. Li, Nano Letters 11 (2011) 2538.
[9] L.M. Xie, X. Ling, Y. Fang, J. Zhang, Z.F. Liu, Journal of the American Chemical Society 131 (2009) 9890.
[10] X. Ling, L.M. Xie, Y. Fang, H. Xu, H.L. Zhang, J. Kong, M.S. Dresselhaus, J. Zhang, Z.F. Liu, Nano Letters 10 (2010) 553.
[11] W. Ren, Y.X. Fang, E.K. Wang, ACS Nano 5 (2011) 6425.
[12] J. Lee, K.S. Novoselov, H.S. Shin, ACS Nano 5 (2011) 608.
[13] S. Sun, P. Wu, Physical Chemistry Chemical Physics 13 (2011) 21116.
[14] N. Kim, M.K. Oh, S. Park, S.K. Kim, B.H. Hong, Bulletin of the Korean Chemical Society 31 (2010) 999.
[15] G. Goncalves, P.A.A.P. Marques, C.M. Granadeiro, H.I.S. Nogueira, M.K. Singh, J. Gracio, Chemistry of Materials 21 (2009) 4796.
[16] J. Wang, X.C. Dong, R. Xu, S.Z. Li, P. Chen, M.B. Chan-Park, Nanoscale 4 (2012) 3055.
[17] A. Otto, I. Mrozek, H. Grabhorn, W. Akemann, Journal of Physics: Condensed Matter 4 (1992) 1143.
[18] A.N.J. Persson, K. Zhao, Z.Y. Zhang, Physical Review Letters 96 (2006) 207401.
[19] A.P. Liu, J.Q. Zhu, J.C. Han, H.P. Wu, C.Z. Jiang, Electrochemistry Communications 10 (2008) 827.
[20] F.X. Liu, Z.S. Cao, C.J. Tang, L. Chen, Z.L. Wang, ACS Nano 4 (2010) 2643.
[21] T. Bhuvana, G.V.P. Kumar, C. Narayana, G.U. Kulkarni, Nanotechnology 18 (2007) 145702.
[22] A.P. Liu, E.J. Liu, G.C. Yang, N.W. Khun, W.G. Ma, Pure and Applied Chemistry 82 (2010) 2217.
[23] W.S. Hummers, R.E. Offeman, Journal of the American Chemical Society 80 (1958) 1339.
[24] N.I. Kovtyukhova, P.J. Ollivier, B.R. Martin, T.E. Mallouk, S.A. Chizhik, E.V. Buzaneva, A.D. Gorchinskiy, Chemistry of Materials 11 (1999) 771.
[25] H.L. Guo, X.F. Wang, Q.Y. Qian, F.B. Wang, X.H. Xia, ACS Nano 3 (2009) 2653.
[26] L.H. Tang, Y. Wang, Y.M. Li, H.B. Feng, J. Lu, J.H. Li, Advanced Functional Materials 19 (2009) 2782.
[27] Y.G. Zhou, J.J. Chen, F.B. Wang, Z.H. Sheng, X.H. Xia, Chemical Communications 46 (2010) 5951.
[28] K. Vinodgopal, B. Neppolian, I.V. Lightcap, F. Grieser, M. Ashokkumar, P.V. Kamat, Journal of Physical Chemistry Letters 1 (2010) 1987.